

## **Failure Mechanism of Pure Epoxy Coating in Near-Neutral Solution Focusing on Coating/Metal Interfaces**

*Chao Yang<sup>1,2,\*</sup>, Guanjun Wang<sup>2</sup>, Qing Han<sup>2</sup>, Haibo Liu<sup>2</sup>, Anquan Wang<sup>2</sup>, Liang Sun<sup>2</sup>*

<sup>1</sup> Postdoctoral Scientific Research Workstation of Shengli Oilfield Company, Dongying, 257000, China;

<sup>2</sup> Technology Inspection Center of Shengli Oilfield, SINOPEC, Dongying, 257000, China

\*E-mail: [yangchao201001@163.com](mailto:yangchao201001@163.com)

*Received: 30 September 2020 / Accepted: 24 December 2020 / Published: 31 January 2021*

Electrochemical impedance spectroscopy (EIS) can provide a rapid and convenient method for evaluating the coatings' anti-corrosion performance, especially for analyzing the evolution of water diffusion. However, due to the coating/metal interfaces' limitation, the electrochemical reaction at interfaces is still not elucidated. Therefore, focusing on coating/metal interfaces, this paper investigates the coating failure mechanism on the coated X80-matrix with pure DGEBA coatings and the formation process of  $\text{Fe}_3\text{O}_4$  at interfaces.

**Keywords:** Epoxy coating; X80-matrix; Near-neutral;  $\text{Fe}_3\text{O}_4$ ; Cathodic protection

### **1. INTRODUCTION**

Organic coatings are widely used in the anti-corrosive protection of buried pipelines. These coatings isolate the pipelines from corrosive media and enhance the efficiency of the cathodic protection. However, the coating's failure caused by the corrosive media diffusion could also be severe, being a hot research topic for a long time, especially focusing on the electrochemical reaction at coating-metal interfaces [1].

Generally, the hydrogen bonds formed by water molecules and polymers are more stable than the coating-metal bond. Therefore, when water molecules reach the coating/metal interface, the fracture of the coating-metal bond occurs, causing the coating delamination [2-4]. However, in the study of Nazarov et al. [5], the reversibility of the coating-metal bonding bond on the interface was proved. Similarly, Leng et al. [6,7] used FTIR to prove that even a large number of water molecules gathered on the interface, the delamination of coating-metal system would not take place. Therefore, the electrochemical reaction process at the interface is the main cause of coating failure [8,9].

Electrochemical impedance spectroscopy (EIS) provides a rapid and convenient method for evaluating the coatings' anti-corrosion performance, where the fitted equivalent circuits can represent the changes of related parameters (such as coating layer capacitors or resistors) and then further analyze the failure behaviors. Because of the complexity of the coating structure and composition as well as the limitation of the coating/metal interfaces, so far, a large number of publications have used electrochemical tests to describe the changes of electrochemical parameters in the process of immersion, and then described the process of coating failure from a macro point of views such as the maximal phase angle and time constant.

However, the researches focusing on the failure of the coatings caused by corrosive media diffusion still have their limitations: (1) the relationship between fitted parameters from EIS and the influence of the corrosive medium on the physical/chemical properties of the coatings is not well-established, which leads to the inconsistency in the selection of equivalent circuits and the determination of key factors in the failure behavior of the coatings. (2) Due to the coating/metal interfaces' limitation, it is challenging to analyze the electrochemical reactions at interfaces directly.

Therefore, in this paper, pure DGEBA epoxy coating applied on X80-matrix was used as the main sample to explore the 3 wt.% NaCl solution's diffusion process. Focusing on coating-metal interfaces, this paper targeted to explore the failure mechanism of epoxy coatings in near-neutral solutions using an electrochemical method (EIS).

## 2. EXPERIMENTAL SETTINGS

### 2.1 Samples

Working electrodes used in this work were obtained from an X80-matrix sheet. The steel samples were sliced into  $25 \times 25 \times 2$  mm<sup>3</sup> cubes, where the fringe effect was ignored [10], and they were embedded in epoxy resin, leaving a working area of  $25 \times 25$  mm<sup>2</sup>. The specimen preparation was controlled carefully to ensure that no grooves and bubbles were generated at the epoxy/steel interface. The specimen's working surface was subsequently ground with sandpapers (800 and 1000 grit), cleaned by distilled water and methanol, and dried [11].

The experimental coating was a sample of DGEBA coating produced by Anhui Wuhu. The weight ratio of epoxy resin to curing agent was 10:1, and the density was 1.28 g/cm<sup>3</sup>. The coating was applied on the surface of the X80-matrix ( $25 \times 25$  mm<sup>2</sup>) by a hand brush and cured for 7 days at room temperature (25 °C). The coating sample thickness was determined by QNIX8500 gauge through the five-point sampling method to the final  $25 \pm 5$  μm with a glass transition temperature of  $T_g = 123$  °C.

### 2.2 Electrochemical test

The electrochemical parameters were obtained by equivalent electric circuits by commercial software of "ZimpWin" software. The test solution was formed by NaCl and deionized water, and glacial acetic acid and hartshorn were used to adjust the pH of the test solution.

The reference electrode was positioned close to the electrode surface ( $\leq 2\text{mm}$ ). Thus, the effect of ohmic drop on the potential measurement was negligible.

EIS measurements were quantified in the nominal frequency range of  $10^5\text{--}10^{-2}\text{ Hz}$ , and all experiments were carried out in constant temperature-humidity chamber "GDJS-408" at temperature  $25\text{ }^\circ\text{C}$ . The electrochemical parameters were obtained by equivalent electric circuits, using "ZimpWin" software.

### 3. RESULTS AND DISCUSSION

#### 3.1 Analysis of open-circuit potential ( $E_{OCP}$ )

Fig.1 shows the changes in the open-circuit potential ( $E_{OCP}$ ) curves. The variation of the  $E_{OCP}$  curve could be divided into four stages:

(i) The first stage was found to be in the range of 0~3 h, where the coating's anti-corrosion performance gradually decreased due to the diffusion of the electrolyte solution, showing an increasing corrosion tendency [12-14] with a decreasing  $E_{OCP}$  of  $-0.710\rightarrow-0.728\text{ V}$ .

(ii) In the second stage (between 4~38 h), the  $E_{OCP}$  decreased slightly ( $-0.728\rightarrow-0.730\text{ V}$ ). Relevant studies suggested that in different coating systems, the time for the corrosive solution to reach the coating/metal interface is about 7~8 h [15]. Therefore, in this stage, the cause of the slight decrease in  $E_{OCP}$  can be attributed to the corrosive medium reaching the coating/metal interface to form the double electrical layer.

(iii) The third stage was between 38~104 h, where the  $E_{OCP}$  decreased significantly ( $-0.730\rightarrow-0.750\text{ V}$ ). Under these conditions, the double electrical layer at the coating/metal interface was formed, suggesting that the coatings' micro-porous diffusion paths were established. Therefore, a large amount of solution entered into the coating, leading to the epoxy coatings' degradation failure behavior [16].

(iv) In the fourth stage (104~177 h), the  $E_{OCP}$  increased and remained unchanged. Since the building of a large number of diffusion channels, the corrosive medium reached the coating/metal interface to accelerate the electrochemical reaction. Afterward, the corrosion products at interfaces diffused reversely into the epoxy coatings to block the diffusion paths, illustrated by the increase of  $E_{OCP}$  [17-19]. However, some researchers say that the increase of  $E_{OCP}$  in this stage may be caused by the interaction of water and functional groups of the epoxy coatings, increasing cross-linking density. This explanation was linked to DGEBA epoxy coatings' characteristics, where the penetration of the water molecules into the coatings may lead to the aggregation of small molecular fragments to form a long polymer chains and then cause the increase of cross-linking density [20,21].

When the immersion time was higher than 1000 h, the epoxy coating was completely stripped from the metal, and the metal was directly exposed to the corrosive medium. In this case, the  $E_{OCP}$  decreased until it remained unchanged ( $-0.77\text{ V}$ ), which was equal to the  $E_{OCP}$  of the uncoated X80 steel in 3 wt.% NaCl solution [22].

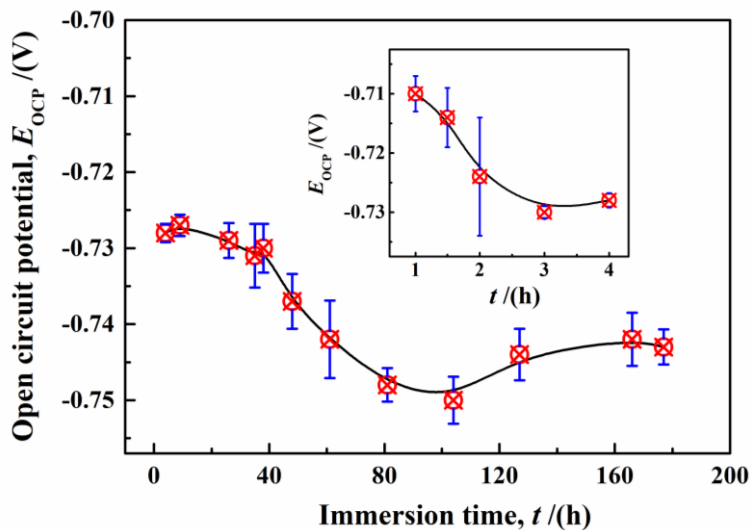


**Figure 1.** Change of open circuit potential of coated X80-matrix in 3 wt.% NaCl solution (immersion time of 0~177 h, temperature - 25 °C)

### 3.2 Analysis of electrochemical impedance spectroscopy (EIS)

Generally speaking, in the initial stage of water diffusion, the coating behaved as a well-performing capacitor to block the entering water, as the Nyquist diagrams showed a "standard" arc of capacitive behavior [23], which was far from the curve tested in this paper.

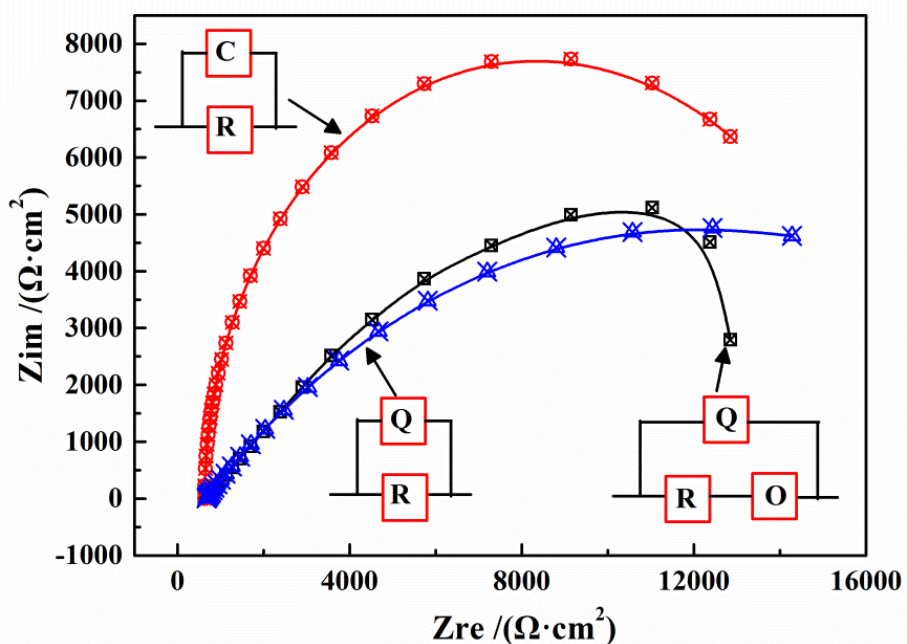


**Figure 2.** Comparison of different equivalent circuit of Nyquist diagram of coated X80-matrix in 3 wt.% NaCl solution (immersion time of 15 min, temperature - 25 °C): (QR), (CR) and (Q(RO))

Fig.2 shows the comparison between different fitted and measured curves at 15 min. Assuming that the coating systems were uniform, their equivalent circuit should be (RC) a series of red curve circuits. Considering the coatings' dispersion effect, the constant phase Angle element  $Q$  was used to replace the pure capacitor  $C$ , in which its equivalent circuit was the (QR) series circuit in the blue curve. However, the test curve in this paper was Q(RO) in black, which the main character was different from the (RC) and (QR). At the high frequency of 10<sup>5</sup> Hz, the imaginary impedance deviated from (QR), reflecting a blocked ion diffusion process. Meanwhile, the error of Q(RO) was less than 3%. Therefore, Q(RO) was selected in the initial stage of water diffusion to describe the water molecules' finite-layer diffusion process in coatings.

The finite layer diffusion element ( $O$ ) was applied to describe the resistance of the coatings to water diffusion, which can be expressed as follows [24]:

$$Z_0 = \frac{1}{Y_0 \sqrt{j\omega}} \tanh(B\sqrt{j\omega}) \quad (1)$$

Where,  $Y_0$  was the capacitance of finite layer diffusion element in F/cm<sup>2</sup> and  $B$  was the index.

The following equation can express the diffusion impedance in a finite layer:

$$R_w = B/Y_0 \quad (2)$$

Therefore, the equivalent resistance can be described as follows:

$$R = R_p + R_w \quad (3)$$

The EIS investigations of coated X80 steel in 3 wt.% NaCl solution at 20 °C were carried out. The diffusion process of water in coatings can be divided into three stages: (i) the diffusion of water in coatings; (ii) the formation of the double electrical layer at coating/metal interface and the (iii) electrochemical reaction at coating/metal interfaces. The EIS curves are presented in Fig.3.

In the initial stage (0~4 h), there was only one capacitive arc in the Nyquist diagram and a "peak" in logf-φ curve, suggesting a constant time to describe the water diffusion in micro-pores. Therefore, the equivalent circuit was  $R_s(Q_c(R_pO))$ :  $R_s$  as solution resistance,  $Q_c$  as coating capacitance,  $R_p$  as polarization resistance and  $O$  as the limited diffusion layer capacitance.

With further diffusion of water, in the second stage (9~26 h), the imaginary impedance at 10<sup>5</sup>Hz in the Nyquist diagram increased gradually to tend to (QR) series circuit at 9 h, where the water reached the coating/metal interface, and the diffusion paths in the coating were established, suggesting the disappearance of the physical shielding effect of the coatings [25]. However, since the water molecules had just arrived on the coating/metal interface, the water on the interface was not expanded, and the double electric layer was not formed. Therefore, it was mainly the double electric layer formation process present until 26 h. Therefore, the equivalent circuit was  $R_s(Q_c(R_c(C_{dl}R_{ct}))$ :  $R_s$  as the solution resistance,  $Q_c$  as the coating capacitance,  $R_c$  as the coating resistance,  $C_{dl}$  as the double-layer capacitance and  $R_{ct}$  as the charge transfer resistance.

In the third stage (35~177 h), once the electrochemical reaction at interfaces took place, the Nyquist diagrams showed small capacitance characteristics at high frequencies and large capacitance at low frequencies. Considering the single-molecule coating adopted in this paper, the coating was considered to be uniform. Therefore, the equivalent circuit was described as the series circuit of the electric double layer and coatings. As the diffusion paths were fully established, the electrochemical

reactions at coating/metal interfaces were affected by the coatings' nature, so the  $Q_{dl}$  was placed forward to replace the pure capacitance ( $C_{dl}$ ).

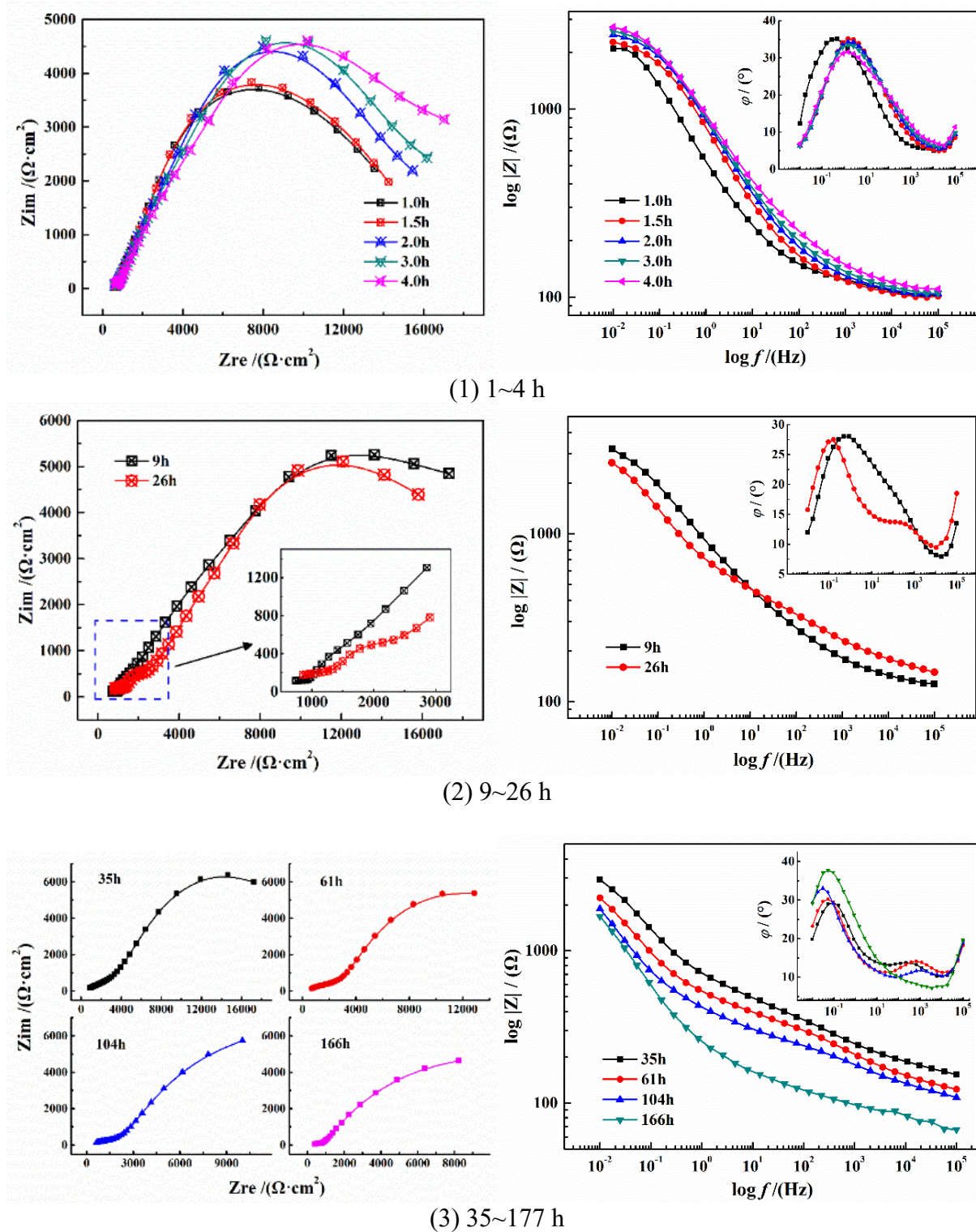


**Figure 3.** EIS analysis of coated X80-matrix in 3 wt.% NaCl solution in 3 wt.% NaCl solution (immersion time of 1~177 h, temperature - 25 °C)

Finally, the equivalent circuit of  $R_s(Q_cR_c)(Q_{dl}R_{ct})$  was established -  $R_s$  as solution resistance,  $Q_c$  as coating capacitance,  $R_c$  as coating resistance,  $Q_{dl}$  as electric double-layer capacitance,  $R_{ct}$  as the charge transfer resistance.

(1) *The diffusion of water molecules in coatings in the initial stage (immersion time of 0~4 h)*

Fig.4 shows the variation of the coating capacitance ( $Q_c$ ), equivalent resistance ( $R$ ), index of  $Q$  ( $n$ ) and polarization resistance ( $R_p$ ) in immersion time of 1~4 h. The results showed that the  $Q_c$  decreased while the diffusion values of  $R_w$  and  $R_p$  increased, which phenomena contradict the traditional view that the coating degraded due to the water diffusion, showing an increasing capacitance and a decreasing resistance. Although the experimental phenomena in this paper were already reported [26], the phenomena were assigned to the water leading to an increasing cross-linking density of the coatings. The water diffusing into the coatings promoted the movement of macromolecule chains, resulting in more adsorption sites between the polymer chains to enhance the cross-linking density.

The conclusion about the increase of cross-linking density of the coating caused by water diffusion can be confirmed by two other parameters of  $n$  and  $R_p$ , as shown in Fig.4. As water diffused, with the diffusion process's progress,  $n$  decreased from 0.42 ( $t=1.0$  h) to 0.18 ( $t=4.0$  h), tending to a resistance characteristic. Meanwhile,  $R_p$  increased from  $196.9 \Omega \cdot \text{cm}^2$  to  $1029 \Omega \cdot \text{cm}^2$ , showing that the water molecules promoted the further cross-linking between coating chains. However, the time constant of  $\tau = Q \cdot R \approx 0.965$  s remained basically unchanged, indicating that there was only a water diffusion process in this stage.

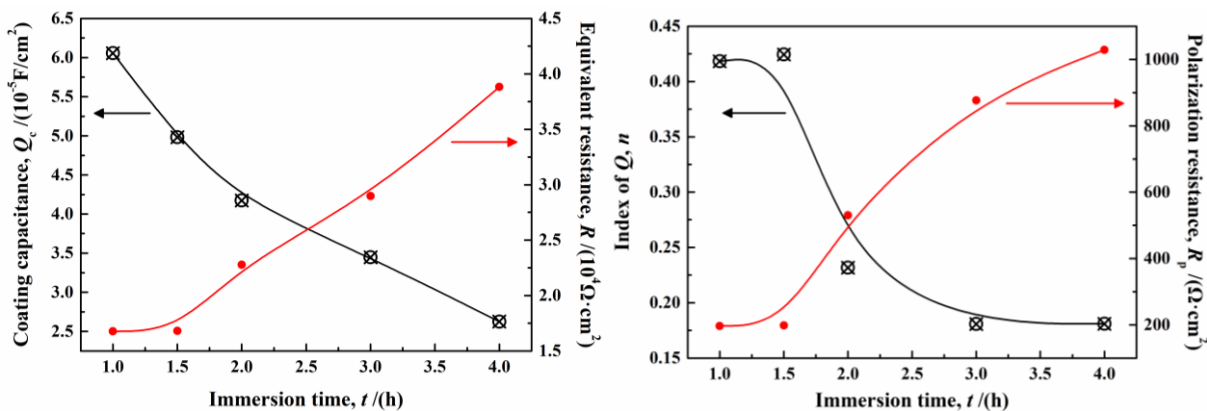


**Figure 4.** Changes of coating capacitance ( $Q_c$ ), equivalent resistance ( $R$ ), index of  $Q(n)$  and polarization resistance ( $R_p$ ) of coated X80-matrix in 3 wt.% NaCl solution (immersion time of 1~4 h, temperature - 25 °C)

Theoretically, within the tested frequency range ( $10^5$ ~ $10^{-2}$  Hz), as the coatings' phase angle ( $\phi$ ) closer to 90°, a higher waterproof performance can be obtained. However, the maximal  $\phi$  was  $\approx 35^\circ$ , far less than 90°, which seemed to reflect the "poor" waterproof performance of the coatings. Meanwhile,

the maximal phase angle frequency ( $f_{\max}$ ) remained basically unchanged ( $f_{\max}=1.4874$  Hz) during 0~4 h, while the maximal  $\varphi$  gradually decreased by 10.12% ( $35.145^\circ \rightarrow 31.59^\circ$ ). In the log-log|Z| curve, the impedance results presented an inclined line with a slope of about "-1" in  $10^5 \sim 10^{-2}$  Hz. These results all proved that the coatings presented pure resistance characteristics in 0~4 h.

(2) *Formation of the double electrical layer at the coating/metal interface (immersion time of 9~26h)*

According to the Nyquist diagrams, when diffusion time reached 26 h, the charge transfer process occurred at high frequencies. However, the imaginary impedance reduced slightly at  $10^5$  Hz, and the capacitive reactance representing the substance diffusion at a lower frequency slightly changed, indicating that this period behaved as the formation of the electric double layer at coating/metal interfaces. The result was following the results of the analysis of Bode plots. The second time constant representing double-layer capacitance appeared at  $f=126.9$  Hz in the logf- $\varphi$  curve, while the logf-log|Z| curve showed a straight line with a slope of "-1".

Compared with the first stage (0~4 h), the  $Q_c$  increased slightly ( $5.96 \rightarrow 6.06 \times 10^{-5}$  F/cm $^2$ ), equal to the value observed at  $t=1.0$  h. Furthermore, the  $R_c$  increased with the immersion time ( $1580 \rightarrow 2654 \Omega \cdot \text{cm}^2$ ), showing a further cross-linking process.

Fig.5 shows the variation of the capacitive reactance characteristics at high-frequencies over immersion time. From the analysis discussed above, it can be observed that the second stage (9~26 h) was mainly described with the formation of the electric double layer at the coating/metal interfaces. With the increase of the immersion time, the capacitive reactance at high frequencies changed little during 26~46 h, meaning that the electric double layer formation was completed at  $\approx 26$  h.

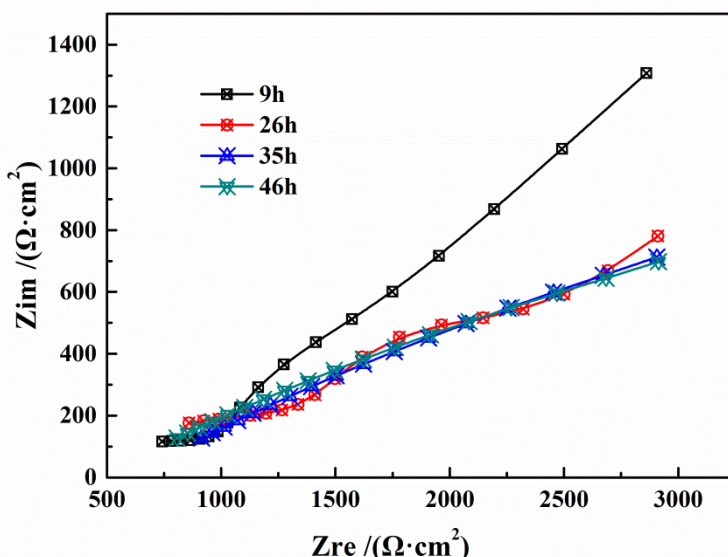


**Figure 5.** Change of high-frequency capacitance reactance arc of coated X80-matrix in 3 wt.% NaCl solution (immersion time of 9~46 h, temperature - 25 °C)

## (3) Electrochemical reaction at coating/metal interfaces in immersion time of 35~177 h

As the water diffusion went on, capacitance-resistance characteristics at high frequencies gradually disappeared. Meanwhile, the logf-log|Z| curve was divided into two sections by the frequency  $f=1$  Hz in Bode plots, representing the double electric layer at the high-frequency area and the coatings at low frequency, respectively. In the range of  $10^5\text{--}10^{-2}$  Hz, the impedance of material diffusion ( $f=10^{-2}$  Hz,  $|Z|=2923\rightarrow1680\ \Omega$ ) and the charge transfer resistance ( $f=10^5$  Hz,  $|Z|=154\rightarrow67\ \Omega$ ) decreased gradually with the immersion time, characterized by the degradation process of the coating/metal system. Therefore, the two aspects could be analyzed in detail as follows.

## a) Electrochemical reaction at coating/metal interfaces

Fig.6 shows the variation of capacitance characteristics at high frequency. As the water diffusion continued, the capacitive reactance arc at interfaces gradually reduced, as the capacitance characteristics (imaginary impedance,  $Z_{im}$ ) and the resistance characteristics (real impedance,  $Z_{re}$ ) in the time of 35~104 h decreased ( $Z_{re}=615\rightarrow409\ \Omega\cdot\text{cm}^2$ ,  $Z_{im}=2159\rightarrow1600\ \Omega\cdot\text{cm}^2$ ). However, at 166 h,  $Z_{re}=58\ \Omega\cdot\text{cm}^2$  and  $Z_{im}=403\ \Omega\cdot\text{cm}^2$ , indicated that the falling rate in 104~166 h was enlarged by about 300%.

At high-frequency, the logf- $\varphi$  curve showed similar characteristics between 35~166 h. Within 35~104 h, the maximal  $\varphi$  decreased from  $13.7^\circ$  to  $11.7^\circ$ , while the  $f_{max}$  increased from 221 Hz to 1172Hz. At 166 h, the peak value of the high frequency basically disappeared.

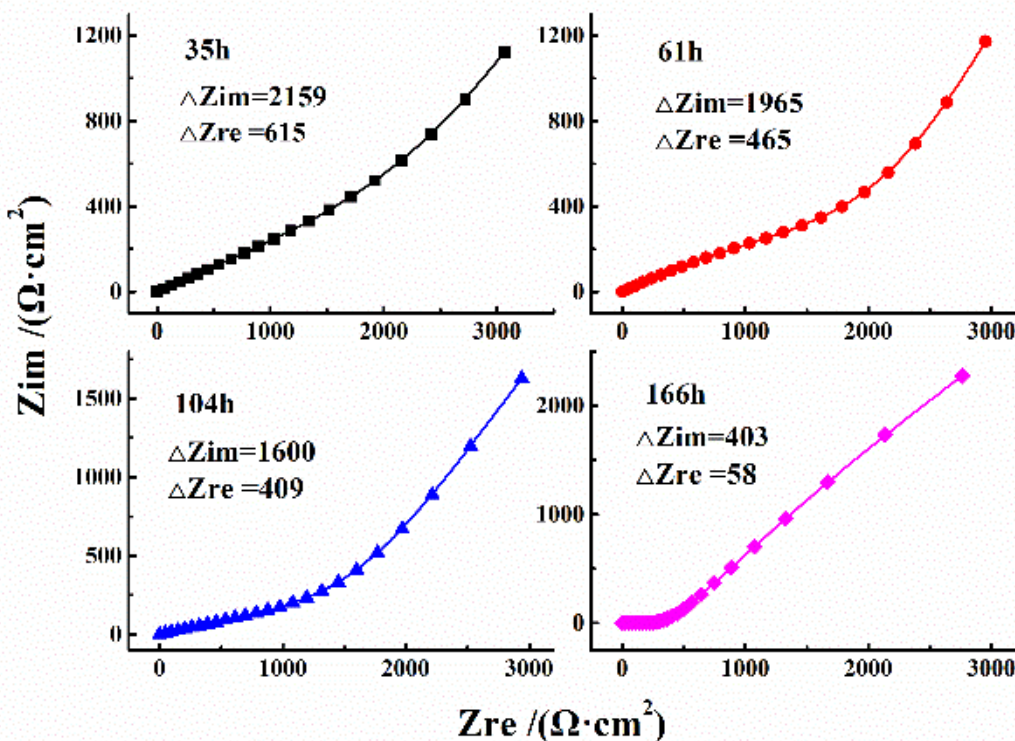


**Figure 6.** Change of high-frequency capacitance reactance arc of coated X80-matrix in 3 wt.% NaCl solution (immersion time of 37~177 h, temperature - 25 °C)

Fig.7 shows the changes of double-layer capacitance ( $Q_{dl}$ ) and charge transfer resistance ( $R_{ct}$ ). Both values showed a trend of increase first (35~104 h) and decreased between 104~166 h. At 35~104h, due to the increase of the concentration gradient, the double-layer thickness was compressed, leading to an increasing of the  $R_{ct}$  value. However, at 104~166 h, the macro phase at coating/metal interfaces was developed, meaning that the double-layer disappeared, and the bubble phenomenon of the coatings was heightened. At this time, it can be theoretically considered that the double-layer thickness increased with the decrease of  $Q_{dl}$  and  $R_{ct}$ .

### b) Decrease of anti-corrosion performance of the coatings

In the low-frequency region, the maximal  $\varphi$  increased from  $29.4^\circ$  to  $37.1^\circ$ , while the corresponding  $f_{max}$  decreased from 0.09 Hz to 0.03 Hz, which indicated that the material diffusion process dominated the whole process.

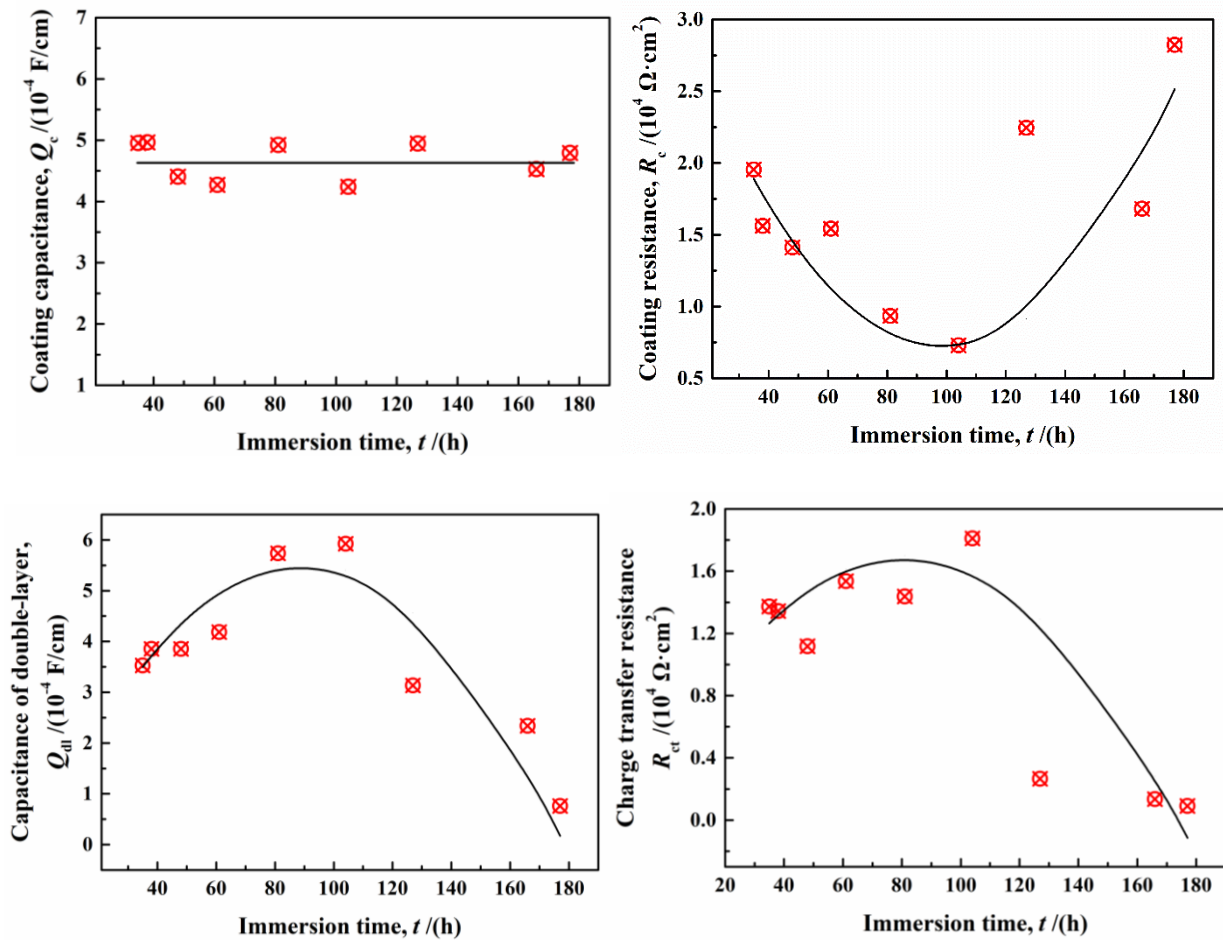


**Figure 7.** Changes of coating capacitance ( $Q_c$ ), coating resistance ( $R_c$ ), capacitance of double-layer ( $Q_{dl}$ ) and charge transfer resistance ( $R_{ct}$ ) of coated X80-matrix in 3 wt.% NaCl solution (immersion time of 37~177 h, temperature - 25 °C)

Accordingly, the diffusion paths within the coatings until 26 h were established, which meant that the further diffusion could not affect the changes of the physical structure of the coating itself, so

the coating capacitance was unchanged ( $Q_c=4.67\times10^{-4}$  F/cm<sup>2</sup>). However, in the third stage (104~166 h), the coating resistance ( $R_c$ ) presented the rules of first increase (35~104 h) and subsequent decrease (104~166 h). The main reasons involved two aspects: (1) Depending on the well-defined diffusion paths, a large number of ions diffused into the coatings, inducing a decrease of the  $R_c$  value; (2) The electrochemical reaction at interfaces was intensified due to the presence of the ions, and then higher amount of corrosion products diffused inversely into the coatings and accordingly blocked the diffusion paths, increasing the  $R_c$ . The results of this analysis were following the value of  $E_{OCP}$ .

### 3.3 Analysis of coating failure due to interfacial electrochemical reactions

In the near-neutral solution (3 wt.% NaCl), when the corrosive medium reached the coating/metal interface, the anode activated the metal corrosion process ( $\text{Fe}\rightarrow\text{Fe}^{2+}+2\text{e}^-$ ), and the cathode performed the  $\text{O}_2$  depolarization process ( $\text{O}_2+2\text{H}_2\text{O}+4\text{e}^-\rightarrow4\text{OH}^-$ ). In this case, the alkalinization and the corrosion products at interfaces destroyed the coating-metal bond, which accelerated the coatings' delamination. Furthermore, due to the limitation of the coating-metal interface, once the  $\text{O}_2$  at the interfaces was exhausted, it was extremely difficult to replenish  $\text{O}_2$ , thus developing an oxygen concentration cell. Under these circumstances, the metal at interfaces worked as an anode during the corrosion process. At the same time, due to the hydrolysis of  $\text{Fe}^{2+}$  ( $\text{Fe}^{2+}+2\text{H}_2\text{O}\rightarrow\text{Fe}(\text{OH})_2+2\text{H}^+$ ), the pH at interfaces changed from alkaline to acidic [27], which accelerated the dissolution of the metal. The oxygen concentration gradient formation promoted corrosion products' aggregation at the interface, and the corrosion products overflowed through the micro-pore diffusion paths, covering the surface of the sample.

The fractal dimension ( $D_f$ ) was used to describe the coating-metal interfaces [28,29]: the higher roughness induced a greater fractal dimension. In EIS analysis, the index ( $n$ ) of constant phase angle element ( $Q$ ) reflected the material-interface heterogeneity related to the fractal geometry, as shown in Eq.(4). In this paper, the fractal dimension can reflect the degree of corrosion reaction at interfaces and preliminarily determine the time of electrochemical reaction.

$$D_f = \frac{1}{n} + 1 \quad (4)$$

Fig.8 shows the changes in fractal dimensions ( $D_f$ ) in immersion time of 1~177 h. The whole curve was divided into three stages. (i) During the first stage (0~4 h), the corrosive medium entered into the coatings, leading to increased inhomogeneity of the coatings, manifested as the increase of fractal dimension. (ii) In the second stage (9~26), the corrosive stage had reached the coating/metal interfaces to form a double-layer; therefore, the fractal dimension basically remained unchanged. (iii) In the final (35~166 h), the fractal dimension increased rapidly in 35~38 h and then decreased sharply after 48 h. This behavior occurred as the electrochemical reaction locally began to damage the metal interface's integrity after 35 h, and subsequently, the electrochemical reaction occurred at whole interfaces. Therefore, the fractal dimension firstly reduced rapidly and then increased a little linearly ( $R^2=0.823$ ).

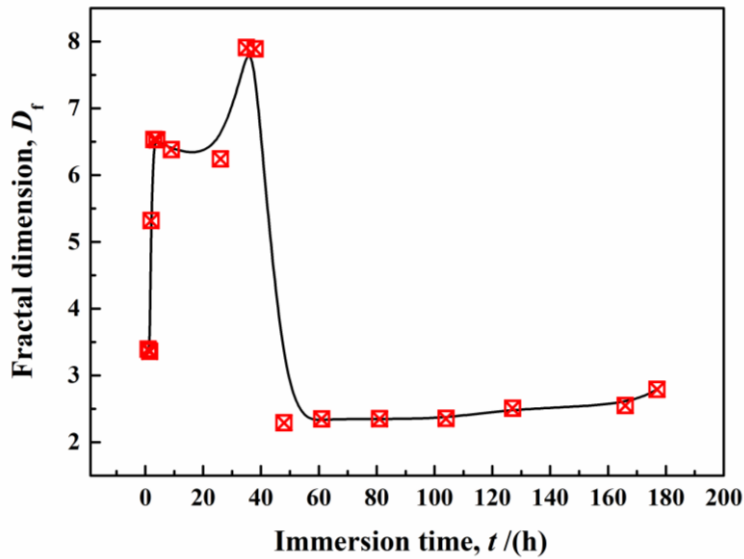


**Figure 8.** Change of fractal dimension of coated X80-matrix in 3 wt.% NaCl solution (immersion time of 1~177 h, temperature - 25 °C)

Fig.9 shows the corrosion mechanism at coating/metal interfaces.

(i) When corrosive medium (including  $H_2O/Na^+/Cl^-/O_2$ ) reached the coating/metal interfaces, the anodic process was dominated by the dissolution of metal ( $Fe \rightarrow Fe^{2+} + 2e^-$ ), and the cathode was the place of the depolarization process of oxygen ( $O_2 + 2H_2O + 4e^- \rightarrow 4OH^-$ ). At this time, the pH at the interface increased and then destroyed the coating-metal bond.

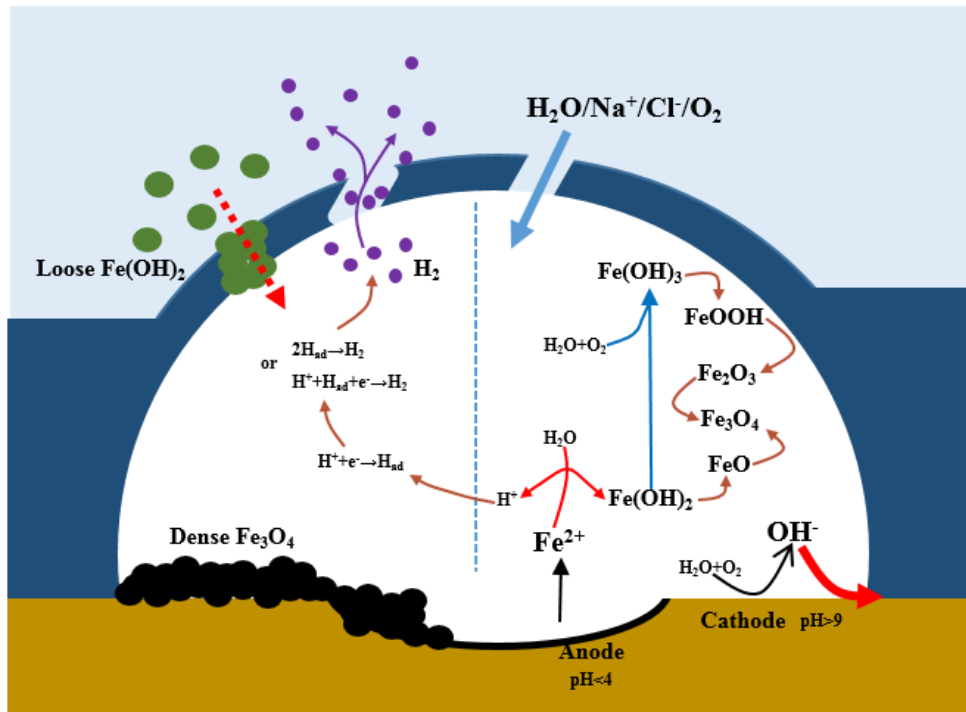


**Figure 9.** Corrosion mechanism at coating/metal interfaces in near-neutral solution

(ii) When the oxygen on the interface was exhausted, an oxygen concentration gradient was formed, accelerating the metal-matrix's corrosion. Meanwhile, the  $\text{Fe}^{2+}$  promoted  $\text{H}^+/\text{H}_{\text{ad}}$  combined to generate  $\text{H}_2$ , leading to a macroscopic bubble phenomenon on the coatings' surface. The effect of the immediate corrosion product ( $\text{Fe(OH)}_2$ ) on the failure of the coating was mainly reflected in two aspects: a) a part of  $\text{Fe(OH)}_2$  reached the coating surface via the diffusion paths and then formed a red-brown precipitate -  $\text{Fe(OH)}_3$ ; b) the other part of the  $\text{Fe(OH)}_2$  transformed into a dense black  $\text{Fe}_3\text{O}_4$  [30].

#### 4. CONCLUSION

In this paper, the failure process of the epoxy coatings in a near-neutral solution was analyzed by electrochemical experiments. The main conclusions were as follows:

(i) In a near-neutral environment, the electrochemical reactions at coating/metal interfaces were prerequisites for the coating failure. Once the corrosive medium reached the interfaces, the electrochemical reaction promoted the destruction of the coating/metal bond to accelerate the delamination and destroy the physical structure of the coatings due to the corrosion products entering the coatings.

(ii) Focusing on the electrochemical reaction at interfaces, the dynamic mechanism was put forward in a near-neutral solution, especially for the formation reaction of the dense  $\text{Fe}_3\text{O}_4$ .

#### References

1. C. Yang, X. Xing, Z.L. Li, and S.X. Zhang, *Polymers-Basel*, 12 (2020) 138.
2. C.F. Dong, A.Q. Fu, X.G. Li, and Y.F. Cheng, *Electrochim. Acta*, 54 (2008) 628.
3. B. Wessling, and J. Posdorfer, *Electrochim. Acta*, 44 (1999) 2139.
4. A. Miszczyk, and T. Schauer, *Prog. Org. Coat.*, 52 (2005) 298.
5. A. Nazarov, and D, *Electrochim. Acta*, 49 (2004) 2955.
6. A. Leng, H. Streckel, and M. Stratmann, *Corros. Sci.*, 41 (1998) 547.
7. J. Carrasco, A. Hodgson, and A. Michaelides, *Nat. Mater.*, 11 (2012) 667.
8. A. Leng, H. Streckel, and M. Stratmann, *Corros. Sci.*, 41 (1998) 579.
9. A. Leng, H. Streckel, and M. Stratmann, *Corros. Sci.*, 41 (1998) 599.
10. L.V.S. Philippe, S.B. Lyon, C. Sammon, and J. Yarwood, *Corros. Sci.*, 50 (2008) 887.
11. L.Y. Xu, X. Su, Z.X. Yin, Y.H. Tang, and Y.F. Cheng, *Corros. Sci.*, 61 (2012) 215.
12. Y.T. Lin, T.M. Don, C.J. Wong, F.C. Meng, Y.J. Lin, S.Y. Lee, C.F. Lee, and W.Y. Chiu, *Surf. Coat. Tech.*, 3 (2018) 1128.
13. S.Y. Arman, B. Ramezanladeh, S. Farghadani, M. Mehdipour and A. Rajabi, *Corros. Sci.*, 77 (2013) 118.
14. H. Hayatdavoudi and M. Rahsepar, *J. Alloy. Compd.*, 727 (2017) 1148.
15. B. Ramezanladeh, M.H.M. Moghadam, N. Shohani and M. Mahdavian, *Chem. Eng. J.*, 320 (2017) 363.
16. S.M. Park and M.Y. Shon, *J. Ind. Eng. Chem.*, 21 (2015) 1258.
17. B. Liu, Z.G. Fang, H.B. Wang, and T. Wang, *Prog. Org. Coat.*, 76 (2013) 1814.
18. H. Jeon, J. Park, and M. Shon, *J. Ind. Eng. Chem.*, 19 (2013) 849.
19. S. Zheng, and J. Li, *J. Sol-Gel Sci. Techn.*, 54 (2010) 174.
20. F.T. Shirehjini, I. Danaee, H. Eskandari and D Zarei, *J. Mater. Sci. Technol.*, 32 (2016) 1152.

21. T.H. Yun, J.H. Park, J.S. Kim and J.M. Park, *Prog. Org. Coat.*, 77 (2014) 1780.
22. H.P. Ji, T.H. Yun, K.Y. Kim, Y.K. Song and J.M. Park, *Prog. Org. Coat.*, 74 (2012) 25.
23. K. Schaefer and A. Miszczyk, *Corros. Sci.*, 66 (2013) 380.
24. B.A. Boukamp, *Solid State Ionics*, 20 (1986) 31.
25. H. Marchebois, C. Savall, J. Bernard and S. Touzain, *Electrochim. Acta*, 49 (2004) 2945.
26. X.W. Liu, J.P. Xiong, Y.W. Lv, and Y. Zuo, *Prog. Org. Coat.*, 64(2009)497.
27. R. Hasanov, S. Bilgi, and G. Gece, *J. Solid State Electr.*, 15 (2011) 1063.
28. P. Hammer, F.C. dos Santos, B.M. Cerrutti, S.H. Pulcinelli, and C.V. Santilli, *J. Sol-Gel Sci. Techn.*, 63 (2012) 266.
29. L. Liu, Y. Cui, Y. Li, T. Zhang, and F. Wang, *Electrochim. Acta*, 62 (2012) 42.
30. Y. Hua, S.S. Xu, Y. Wang, W. Taleb, J.B. Sun, L. Zhang, R. Barker, and A. Neville, *Corros. Sci.*, 157 (2019) 382.

© 2021 The Authors. Published by ESG ([www.electrochemsci.org](http://www.electrochemsci.org)). This article is an open access article distributed under the terms and conditions of the Creative Commons Attribution license (<http://creativecommons.org/licenses/by/4.0/>).